Theor Chem Account (2007) 118:881–898
DOI 10.1007/s00214-007-0376-5

REGULAR ARTICLE

The 1-D hindered rotor approximation

Jim Pfaendtner · Xinrui Yu · Linda J. Broadbelt

Received: 2 October 2006 / Accepted: 7 June 2007 / Published online: 24 July 2007

Abstract We offer an overview of the popular one-dimensional (1-D) hindered rotor model that is often used for quantum mechanical treatment of internal rotation. This model is put in context with other methods used for treating anharmonic motions. The 1-D hindered rotor scheme is general for tops of any symmetry and has been used to provide accurate treatment of hindered rotors in a wide range of systems. One obstacle preventing wider use of the model is its lack of incorporation into common electronic structure codes. We have developed an algorithm for consistently treating all tops in a molecule, and we present simple codes which interface with electronic structure codes to provide thermochemical properties (S, C_p, H) of individual species and reactions that have been corrected for internal rotations. Finally, we use this approach to give sensible advice about how the model can be used best. We show that dramatic changes in the reduced moment of inertia do not necessarily cause comparable changes in the properties of individual hindered rotors. We demonstrate that the rotational hindrance potential can be accurately determined using relatively coarse step sizes. Finally, we show that internal rotation in transition states can be treated using a "frozen transition state" approximation at a significant computational savings. We also discuss the relationship between calculated properties of hindered rotors and the choice of method and basis set used.

Electronic supplementary material The online version of this article (doi:10.1007/s00214-007-0376-5) contains supplementary material, which is available to authorized users.

J. Pfaendtner · X. Yu · L. J. Broadbelt (✉)
Department of Chemical and Biological Engineering,
Northwestern University, Evanston, IL 60208-3120, USA
e-mail: broadbelt@northwestern.edu

1 Introduction

Quantum chemistry is rapidly becoming the de facto choice for calculating estimates of thermochemical properties of radicals and molecular species as well as kinetic parameters of chemical reactions for a wide range of systems. The impressive success of density functional theory (DFT) and other ab initio methods in predicting desired properties with sufficient accuracy, the large amount of inexpensive computing power presently available, and the wide availability of user-friendly software such as GAMESS [1] and Gaussian [2] continue to increase the number of practitioners of quantum chemistry. The ever-increasing number of examples of the success of quantum chemistry in addressing problems of practical interest has even motivated research groups who were traditionally experimental to add electronic structure calculations to their arsenal. High-level ab initio studies of real systems are now beginning to offer not only qualitative insights but also quantitative predictions of thermodynamic and kinetic properties.

Although quantitative predictions are available using commercial quantum chemistry software packages, continuous improvement in their accuracy is sought, and often this involves additional calculations and analyses that are beyond those available in a standard menu of choices within the codes. One example of this is the treatment of internal rotations. It has been understood for over 60 years that errors are introduced by applying the harmonic oscillator (HO) approximation to low frequency vibrational modes [3], yet no general procedure is in common use that offers improved treatment of anharmonic molecular vibrations [4]. Treatment of anharmonicity is an area of active research as evidenced by the multitude of approaches presented in the literature to address this problem [4–35]. The method of Ayala and Schlegel [12] has been incorporated into the Gaussian

software packages but offers approximate corrections for hindered rotors that may not provide sufficient accuracy. Truhlar [6] and later McClurg et al. [36] offered a simple prescription for calculating the partition function between the high and low-temperature limits, i.e., the hindered rotor regime. However, these methods are specific to tops whose rotational hindrance potential can be fit to a single cosine function, and many tops in species of practical interest do not fall into this category. At present, accurate treatment of internal rotation still requires substantial manual effort, which can be tedious and time-consuming when large species or studies which include a large number of reactions are of interest. A common approach for the treatment of hindered rotors is to assume uncoupled rotation. This is due to the fact that the exact Hamiltonian is very complicated, and it is impossible to decouple any degrees of freedom exactly except for translational motion. However, accurate thermochemistry and (in many cases) kinetics can be calculated by making the rigid-rotor harmonic oscillator approximation. Accordingly, a common approximation in treating vibrational anharmonicity due to internal rotation is to treat internal rotors with an effective one-dimensional Hamiltonian. While it has been clearly shown that using this assumption may sacrifice accuracy in cases of complicated or highly coupled rotations [26,30], the computational demands introduced by multidimensional treatment of large systems still dictate that the assumption of uncoupled rotations will continue to be invoked in the foreseeable future. In addition, very accurate treatment of rotation–vibration in small, i.e., four atom, systems can be obtained at the expense of second derivative calculations as a function of the internal rotation coordinate [37–41]. However, we omit any detailed discussion and comparison of these methods for practical reasons due to difficulties in their application to larger molecules.

This overview is motivated by our own journey in putting treatment of internal rotations into practice. We discovered that there are no freely distributed codes available that provide research-grade treatment of individual hindered rotations and subsequently incorporate these results into the calculation of properties of entire species or reactions. For example, calculating the properties of pentane requires treatment of the four internal rotations in the molecule. Presently, each internal rotation must be treated separately and its respective contribution to the partition function or thermodynamic properties must be manually counted. Performing all of these steps manually for more than a few internal rotations is very cumbersome and not practical. It is therefore desirable to have a single program that can extract data from existing electronic structure software, perform the internal rotation correction and apply this correction to all individual rotors, and output complete properties, e.g., partition functions and thermodynamic quantities, for entire species or reactions. In addition, to the best of our knowledge, no source exists which describes all of the steps involved in this multistep process in detail; rather the elements must be pulled from a wide array of literature sources.[1] This overview seeks to remedy this by focusing on the following:

1. Review the elements of one-dimensional (1-D) treatment of internal rotations applicable for low to moderate temperatures.
2. Describe how these steps have been formulated into software that is freely available and can be applied to an entire species or chemical reaction.
3. Place the 1-D hindered rotor treatment in context with other approaches for treating anharmonicity and briefly summarize emerging methods for treatment of internal rotations that offer a higher degree of accuracy for more complex rotors.
4. Present several sample calculations that help to explore the impact of various decisions that must be made in the treatment of internal rotation, namely, (1) the correct procedure for treating internal rotation in transition states, (2) what is the relationship between calculated hindered rotor properties and the choice of method/basis set for determining the hindrance potential, (3) correctly establishing a functional form of the hindrance potential, (4) quantifying the ramifications of assuming that the reduced moment of inertia for rotating tops is invariant while undergoing rotation.

2 Treatment of internal rotation using quantum mechanics

Pitzer and Gwinn's [3] seminal work on the general treatment of internal rotation as well as the subsequent works by Pitzer [42] and Kilpatrick and Pitzer [43] are the foundation for many present treatments of internal rotation. Additionally, this literature illustrates the challenges associated with accurate treatment of internal rotation. The essential change from Pitzer and Gwinn's original approach in the last 60 years is the extension to systems in which the quantum mechanical energy levels of 1-D rotations cannot be solved analytically. A common approach presently adopted by many researchers [23,26,27,34,44–47] is to use electronic structure software to calculate minimum energy or transition-state structures, calculate the Hessian and resulting harmonic vibrational frequencies, and finally calculate the partition function and desired thermodynamic properties within the HO approximation. Typically, this entire process is completed within computational chemistry software or associated post-processing codes, e.g., the "*freqchk*" utility of Gaussian 03 [2]. Each internal

[1] The reader is referred specifically to references [33,17], and [9] and references therein for further reading.

rotation is treated, and the HO partition functions and thermodynamic properties are then corrected to (1) remove the contribution of low-frequency vibrations that are hindered/free rotors and (2) include the associated contribution of each internal rotation. We review the procedure for treating hindered rotors within the 1-D approximation.

2.1 The 1-D hindered rotor model

One of the most successful methods for treating internal rotation is the 1-D hindered rotor (1-DHR) model [16,26,48]. In this model, each single bond between polyvalent atoms is treated as an axis of rotation between two counter-rotating tops. The potential energy surface for the rotation is determined by starting at a minimum energy or transition-state structure and then progressively rotating the top over 360°. It is important to note that the assumption of separability implies that all internal coordinates except for the dihedral bond undergoing rotation remain fixed while obtaining the potential energy surface. Experience has shown [47,49] that this results in barriers to rotation that are much too high. Most researchers now obtain the 1-D potential energy surface by holding the dihedral angle for the rotation fixed and then calculating the minimum energy structure using a constrained optimization routine. This process itself indicates that internal rotation is coupled to other motions, and this approximation should be remembered. Additionally, the barriers for internal rotation, i.e., the difference in adjacent maxima and minima in the 1-D PES, can be further improved by performing a rigorous saddle point optimization at each peak obtained during the constrained geometry optimization. The increase in computational cost can be non-trivial due to the second derivative calculations that must be performed; as a result most researchers approximate the barrier for internal rotation as the value obtained by constrained geometry optimization alone. Finally, it is also possible to augment the potential energy surface by including zero-point corrections as a function of theta so that $V(\theta) = \epsilon_e(\theta) + \mathrm{ZPE}(\theta)$. Rigorous calculation of the ZPE of hindered rotors was recently discussed by Ellingson et al. [33]. Regardless of the method in which it was obtained, the energy profile is fit to a trigonometric function and the reduced moment of inertia for the rotating top is calculated from the geometry of the stationary point. Once the potential is obtained, the energy levels for the rotation are obtained by solving a 1-D Schrödinger equation,

$$-\frac{h^2}{8\pi^2 I_{\mathrm{red}}}\frac{\mathrm{d}^2}{\mathrm{d}\theta^2}\Psi + V(\theta)\Psi = E\Psi, \tag{1}$$

where I_{red} is the reduced moment of inertia for the rotating top and $V(\theta)$ is the rotational hindrance potential. The energy levels from this calculation are used to calculate the partition function by direct counting for each internal rotation as a function of temperature,

$$q_{\mathrm{ir}} = \frac{1}{\sigma_{\mathrm{r_i}}}\sum_j g_j \exp\left(-\frac{\epsilon_j}{kT}\right), \tag{2}$$

where $\sigma_{\mathrm{r_i}}$ is the internal symmetry number of the rotating top and g_j is the degeneracy of the jth energy level, ϵ_j. Once the partition function for each internal rotation is known, thermodynamic properties, i.e., *E, S,* and C_p, are easily obtained using standard formulae [50]. A classical treatment for 1-D hindered rotors that is applicable at higher temperatures was given by Pitzer and Gwinn [3]. However, the classical treatment still requires that the hindrance potential, $V(\theta)$, be calculated. Given that the hindrance potential must be calculated for both the classical and quantum mechanical treatment and that the classical 1-D treatment is not applicable at low temperatures, we restrict all subsequent discussion to quantum mechanical treatment of internal rotation.

The computational bottleneck in treating internal rotation comes from performing n constrained geometry optimizations to establish the hindrance potential, where n is the number of steps required to traverse the entire rotation. For a species with m hindered, or internal rotations, there are $n \times m$ constrained optimizations which must be performed to treat the entire species. Obtaining the energy levels for the rotation from Eq. 1 is performed at a fraction of the computational cost compared to actually determining the hindrance potential. An important consideration in defining the four atoms that constitute the dihedral angle is that the potential, $V(\theta)$, can be different depending on which atoms are chosen. Sterically hindered or bulky groups will have more or less interaction depending on whether they are constrained to be in a specific plane as the groups undergo rotation. To try to quantify the impact of this, we examined the backbone rotations in butane and 1,2-dichloroethane. For each species there are nine different ways to define the dihedral plane. Using increments of 30°, we developed nine separate hindrance potentials for each species and compared their relative barrier heights. For these two species, very small differences between the barrier heights (<0.1 kcal/mol) were observed. However, it is important to be aware of this issue. The validity of a given rotational potential can easily be checked by defining the dihedral plane with the larger atoms/groups as well as smaller ones and comparing the two curves obtained. Additionally, this problem could be remedied by performing a saddle point optimization at each peak in the 1-D potential in order to better approximate the true barrier height.

To assist in developing a general algorithmic approach to perform the 1-DHR treatment as has been implemented in our software [51,52],[2] the entire process for a given species

[2] Information about obtaining these scripts can be found at http:\\www.broadbelt.chem-eng.northwestern.edu.

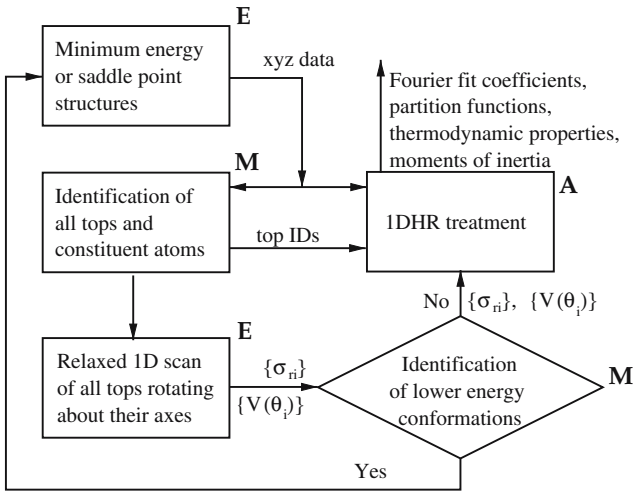

Fig. 1 Flowsheet showing overall process of the 1-DHR treatment. The process begins with a minimum energy or saddle point (e.g., a transition state) structure, and the outputs are the partition functions and thermodynamic properties of each internal rotation for a given species. **E** denotes a step carried out with standard electronic structure software; **M** designates a step that requires manual intervention; **A** signifies that the 1-DHR treatment is automated as implemented in our software

is summarized in the flowchart shown in Fig. 1. The flowsheet shows how information flows beginning with the minimum energy or saddle point (e.g., transition state) structure and terminates with the output of the partition function and respective thermodynamic properties. Steps which are typically completed by researchers using standard electronic structure codes are denoted with an **E**; steps requiring manual input from the user are denoted with an **M**; the 1-DHR treatment is labeled with an **A** reflecting the fact that this step is completed automatically once the user has completed the manual steps. Specifically, the two atoms constituting the axis of rotation for each top, the set of atoms which belong to each rotating top, and the symmetry number for each rotation must be identified as prescribed in the central box on the left hand side of Fig. 1, and the hindrance potential must be inspected to ensure that no other conformations of lower energy exist. The return path denoted in Fig. 1 allows for the case when initial attempts via conventional geometry optimization and even sampling configurational space by the traditional method of starting with different initial geometries did not identify the lowest energy conformation. Although performing constrained, 1-D rotations about all of the rotating tops in a species is certainly not a guaranteed method for obtaining the global minimum energy structure, this approach does sample a large part of conformational space and offers another route to the discovery of other minimum energy structures which may be lower in energy than the starting point. For example, we have recently observed [49] that following the minimum energy path for some intramolecular hydrogen transfer reactions leads to a reactant which is not at the global minimum in electronic energy, i.e., the lowest energy reaction path appears to proceed through an unexpected conformation. A consequence of performing the 1-DHR correction is that low-energy conformers may be naturally detected.

The process represented by the flowsheet in Fig. 1 could be, in principle, embedded directly within the electronic structure code or simply used as a post-processing component for obtaining the desired thermochemical or kinetic properties. For clarity, we have expanded the box denoted "1-DHR" in Fig. 1 into the sub-flowsheet given in Fig. 2. The sub-flowsheet for the 1-DHR treatment clearly shows how information flows through the 1-DHR treatment and shows both the calculations which are required as well as the interdependence (or lack thereof) of these calculations. For each internal rotation in a given species, the sub-flowsheet "1-DHR" is traversed one time. Each component of the "1-DHR" block is briefly expanded upon below.

2.1.1 Reliable fits for hindrance potentials of any form

Pitzer and Gwinn [3] treated symmetric tops whose rotational potentials could be fit to the simple form, $V(1-\cos n\theta)/2$, where V is the barrier height for rotation and n is the number of minima per rotation, i.e., the rotational symmetry number for that top. In reality, only the most simple rotating tops can be described with a single trigonometric function. However, a Fourier series expansion with multiple terms easily fits top rotations of almost any form. The procedure for taking discrete data from a constrained geometry optimization and obtaining a set of coefficients for a Fourier series is very straightforward and briefly described here for reference.

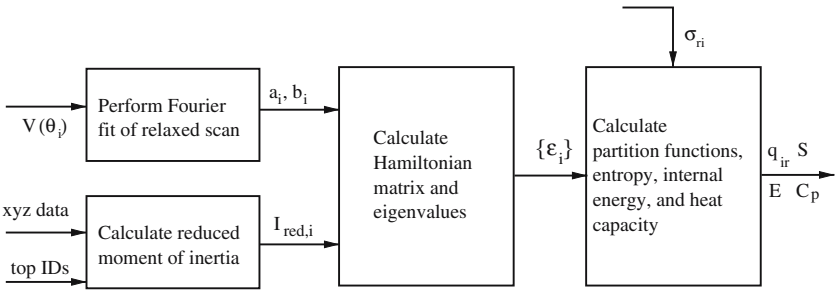

Fig. 2 Flowsheet showing the calculations which are required specifically to calculate the energy levels and thermodynamic properties of each individual internal rotation. For each internal rotation in a given species, the process shown here is repeated

The n-term Fourier expansion can be represented in the following form:

$$V(\theta_j) = \sum_{k=1}^{n} [a_k(1 - \cos\, k\theta_j) + b_k \sin\, k\theta_j]. \tag{3}$$

The coefficients a_k and b_k can be obtained by using the discrete data points ($V(\theta_j)$) obtained from electronic structure calculations and performing a least-squares regression of the overdetermined system:

$$\begin{bmatrix} 1-\cos\,\theta_1 & \sin\theta_1 & \ldots & 1-\cos\,n\theta_1 & \sin\,n\theta_1 \\ 1-\cos\,\theta_2 & \sin\theta_2 & \ldots & 1-\cos\,n\theta_2 & \sin\,n\theta_2 \\ 1-\cos\,\theta_3 & \sin\theta_3 & \ldots & 1-\cos\,n\theta_3 & \sin\,n\theta_3 \\ & & \ldots & & \\ 1-\cos\,\theta_{m-2} & \sin\theta_{m-2} & \ldots & 1-\cos\,n\theta_{m-2} & \sin\,n\theta_{m-2} \\ 1-\cos\,\theta_{m-1} & \sin\theta_{m-1} & \ldots & 1-\cos\,n\theta_{m-1} & \sin\,n\theta_{m-1} \\ 1-\cos\,\theta_m & \sin\theta_m & \ldots & 1-\cos\,n\theta_m & \sin\,n\theta_m \end{bmatrix} \times \begin{bmatrix} a_1 \\ b_1 \\ \ldots \\ a_n \\ b_n \end{bmatrix} = \begin{bmatrix} \varepsilon_1 \\ \varepsilon_2 \\ \varepsilon_3 \\ \ldots \\ \varepsilon_{m-2} \\ \varepsilon_{m-1} \\ \varepsilon_m \end{bmatrix}. \tag{4}$$

The dimensions of the three matices, denoted as A, x and E from left to right, are $m \times 2n$, $2n \times 1$ and $m \times 1$, where n is the number of coefficient pairs and m is the number of energy points in the potential energy scan. The number of coefficient pairs must be lower than the number of energy points if the least squares method is used to solve for the coefficients. In systems in which a large number of points are used, i.e. the step size in scanning the rotation is small, we found that ten terms in the Fourier series (five sine and five cosine terms) fit the calculated data extremely well for all cases that we tested. For test cases in which ten or fewer data points were used to establish the hindrance potential, we typically chose $2n = m - 2$. The coefficient matrix x can be solved as:

$$x = (A^{\mathrm{T}}A)^{-1}A^{\mathrm{T}}E. \tag{5}$$

It is important to note that as n approaches m over-fitting can occur and the functional form obtained from this procedure will give nonsensical values. This can be easily checked by using Eq. 3 and plotting the potential over the entire range, 0–2π. If too many coefficients have been used, the curve will agree with the discrete points $V(\theta_j)$ but not follow the general shape of the potential at intermediate points. Another way to test the quality of the fit is to make sure that the following two conditions are met at $\theta = 0$:

$$\left.\frac{\mathrm{d}V}{\mathrm{d}\theta}\right|_{\theta} = 0, \quad \text{i.e.,} \sum_{k=0} k * b_k = 0, \tag{6}$$

$$\left.\frac{\mathrm{d}^2V}{\mathrm{d}\theta^2}\right|_{\theta} > 0, \quad \text{i.e.,} \sum_{k=0} k * a_k > 0. \tag{7}$$

This is based on $V(0)$ being located at a global minimum.

One question which has not been addressed in the literature is the sensitivity of the hindered rotor partition function (and associated thermodynamic quantities) to the step size used in obtaining the hindrance potential, $V(\theta_j)$, for each rotation. Many researchers have adopted a standard step size of 30° while traversing the rotation of 360° [44,49,53], whereas others use increments as small as 10° [47,54] or even 5° [34] for obtaining the hindrance potential. The relationship between the step size of the hindrance potential and the resulting partition function/thermodynamic properties is further discussed in Sect. 5. Additionally, we build on the results of East and Radom [9] by calculating the hindrance potential using several DFT and MO methods in conjunction with three different basis sets. The impact of the choice of method on the calculated properties is discussed in Sect. 5.

2.1.2 Calculation of the reduced moment of inertia

The next block in Fig. 2 shows the calculation of the reduced moment of inertia. In the limit of a molecule with only one rotation axis, there is an exact reduced moment of inertia that correctly couples both counter-rotation of the two rotating portions, or tops, as well as the internal/external molecular rotation [3,9,42]. In general, the two sides of the molecule are not equally balanced and calculation of an appropriate effective moment of inertia requires consideration of the coupling of internal rotation with total molecular rotation as well as the coupling of the counter-rotation of the two parts of a molecule separated by a rotation axis. There are many different approximations used in determining the reduced moment of inertia that is used in Eq. 1. Ellingson et al. [33] have recently provided a thorough discussion of many alternate approaches to calculating effective moments of inertia. Additionally, East and Radom [9] provided a convenient formalism for distinguishing between these moments of inertia. A popular approximation for the coupling of internal rotation and total molecular rotation was given by Herschbach et al. [55] and discussed further by East and Radom [9]. In the notation of East and Radom, this approximation is $I(2, n)$ where n refers to the degree of coupling between the two counter-rotating tops. The user-specified input is comprised of the structure of the species, the axis of rotation, and the identity

of all the atoms on each side of the molecule (separated by the two atoms defining the twisting bond under consideration).

$$\frac{1}{I^{2,n}} = \frac{1}{I_{\mathrm{L}}^{2,n}} + \frac{1}{I_{\mathrm{R}}^{2,n}}, \tag{8}$$

where the designations L and R in Eq. 8 refer to the fact that the molecule has been separated into two halves (designated "left" and "right", arbitrarily) by the rotation axis for each internal rotation. Each quantity I is the moment of inertia for each side of the species about the axis of internal rotation, which is expressed as:

$$I_{\mathrm{L\,or\,R}}^{2,n} = \sum_i m_i d_i^2, \tag{9}$$

where d_i is the distance from the ith atom in the top to the rotation axis. Equation 9 is a summation only over the atoms in one of the counter-rotating groups, i.e., the "top" and is calculated for the "left" and "right" sides of the molecule. This process is repeated for each internal rotation in a given species in order to calculate all of the effective reduced moments of inertia.

An important consideration is the designation of the axis of internal rotation (the n classification in the notation of East and Radom). If $n = 1$ the axis of rotation is the single bond undergoing rotation. Coupling the counter-rotation of the two sides of the molecule is accomplished through the approximations $n = 2$ (the axis of rotation is parallel to the bond but passes through the center of mass of the smaller of the two rotating tops) and $n = 3$ (the axis of rotation is defined as the line connecting the centers of mass for the two rotating groups). Since each of the successive approximations brings the axis of rotation closer to the heavier atoms in the molecule, we should expect that the reduced moment of inertia will decrease in magnitude, i.e., $I^{2,1} > I^{2,2} > I^{2,3}$. This mode of approximation to the reduced moment of inertia is attractive for species with more than one internal rotation because exact treatment in species with many rotors is extremely complicated. The $I^{2,3}$ approximation has been recommended for use elsewhere [47,56]. We investigated the ramifications of using the different $I^{2,n}$ in Sect. 5.

In addition, there is also a small Coriolis contribution to all effective moments of inertia. This is typically neglected (as has been done in this work), but may become important in cases where the rotating groups are not rigid or the separability approximation breaks down [29,32,57]. Equation 1 implies that I_{red} is not a function of θ and therefore is constant throughout rotation. However, this is not the case for tops that are not rigid while rotating [3,47]. The reduced moment of inertia for a given top can, in principle, be calculated as a function of the rotation angle. It is therefore interesting to probe what effect the assumption that I_{red} is constant has on the calculated properties, which would be expected to be more dramatic as larger molecules are treated. We explore the impact of this assumption quantitatively in Sect. 5.

2.1.3 Obtaining the energy levels of the hindered rotor

Following the scheme in Fig. 2, the hindrance potential (as a Fourier series) and reduced moment of inertia are then used in solving Eq. 1 to obtain the resulting energy levels. One common approach to solve Eq. 1 is to use a grid-based method wherein the Hamiltonian is discretized over the rotation. The eigenvalues and eigenvectors of the resulting diagonal matrix directly give the energy levels and wavefunctions for the rotation. A number of different grid methods have been employed for studying 1-DHR problems [16,58–61]. We have implemented the Fourier grid Hamiltonian (FGH) method of Marston and Balint-Kurti [59–61] that is general for potentials of any form, is easily implemented numerically and has relatively fast convergence. It is therefore an ideal method for solving the 1-D Schrödinger equation when implementing the 1-DHR treatment in a generalized way such as that described here. The convergence of numerical methods for solving Eq. 1 is dependent on the magnitude of the reduced moment of inertia, the shape and size of the rotational potential, and the temperature (for considering convergence of properties like q_{ir} and S_{ir}). We tested a wide range of these parameters and found that in all cases 1,000 grid points were sufficient to converge the energy levels and properties such that increasing the number of grid points changed their values by much less than 1%.

2.1.4 Calculating the properties of each internal rotation

The final block in Fig. 2 is calculation of the partition function and thermodynamic properties of each internal rotation. Once the energy levels for the hindered rotor are known, this step becomes trivial and is completed using standard formulae [50]. One caveat in this step is that for high temperatures or very small barriers, i.e., $kT >> V$, there are so many populated energy levels that a very large basis set must be used. Therefore, in this limit the hindered rotor can be approximated as a free rotor with no loss of accuracy [12,17]. For example, when reporting thermodynamic properties of hydrocarbons the heat capacity is typically reported up to 1,500 K. At this temperature RT is 3 kcal/mol and so for much lower barrier heights or much greater temperatures, a free-rotor description is more appropriate. The free-rotor/hindered-rotor transition has been discussed in detail elsewhere [6,12,36]. While the partition function for hindered rotors is calculated using Eq. 2, the free rotor partition

function can be estimated using the symmetry number, σ_{r_i}, and reduced moment of inertia for the rotation, I_{red} [12]:

$$q_{fr} = \sqrt{\frac{8\pi^3 kT I_{red}}{\sigma_{r_i}^2 h^2}}. \tag{10}$$

Equation 10 is also based on the approximation that the reduced moment of inertia is constant throughout the angle of rotation. The associated thermodynamic properties for hindered rotors calculated in the final block of Fig. 2 are:

$$S_{hr} = k \ln q + \frac{1}{T} \frac{\sum_j g_j \epsilon_j \exp\left(-\frac{\epsilon_j}{kT}\right)}{\sum_j g_j \exp\left(-\frac{\epsilon_j}{kT}\right)}, \tag{11}$$

$$E_{hr} = \frac{\sum_j g_j \epsilon_j \exp\left(-\frac{\epsilon_j}{kT}\right)}{\sum_j g_j \exp\left(-\frac{\epsilon_j}{kT}\right)}, \tag{12}$$

$$Cv_{hr} = \frac{\left(\sum_j g_j \exp\left(-\frac{\epsilon_j}{kT}\right) * \sum_j g_j \frac{\epsilon_j^2}{kT^2} \exp\left(-\frac{\epsilon_j}{kT}\right)\right) - \left(\sum_j g_j \frac{\epsilon_j}{kT^2} \exp\left(-\frac{\epsilon_j}{kT}\right) * \sum_j g_j \epsilon_j \exp\left(-\frac{\epsilon_j}{kT}\right)\right)}{\left(\sum_j g_j \exp\left(-\frac{\epsilon_j}{kT}\right)\right)^2}, \tag{13}$$

whereas the thermodynamic properties of free rotors are:

$$S_{fr} = k\left(\ln q_{fr} + \frac{1}{2}\right), \tag{14}$$

$$E_{fr} = \frac{kT}{2}, \tag{15}$$

$$Cv_{fr} = \frac{k}{2}. \tag{16}$$

Within the framework described here we can easily select a point for the FR/HR transition and use the appropriate formulae accordingly.

2.1.5 Correcting the harmonic oscillator partition function

As stated previously, the common approach in correcting for internal rotation involves first calculating the corresponding partition function and thermodynamic properties within the HO approximation, i.e., using all of the vibrational frequencies, and subsequently removing the contributions (partition functions and thermodynamic properties) of low-frequency vibrations that correspond to internal rotations. One way to carry this out is simply to select the n lowest vibrational frequencies where n is the number of internal rotations treated. This often is an acceptable approach for species which are minimum energy structures. However, in some cases, e.g., transition states, some of the lowest energy vibrations do not correspond to internal rotations. In this case, an internal modes analysis[3] can be used to identify the contribution of various internal coordinates (bending, stretching, torsion) to each harmonic frequency. The internal modes analysis is performed at negligible incremental computational cost once the Hessian is calculated. Therefore, this more rigorous approach is recommended to identify the harmonic frequencies most closely corresponding to each internal rotation. The internal modes analysis also reveals that there can be substantial mixing between various modes when the HO frequencies are calculated. Van Cauter et al. [30] have addressed this in the context of calculated kinetic data for radical addition in polyethylene propagation reactions. They have offered a method for calculating the frequency which corresponds to pure internal rotation, thus improving the 1-DHR correction. Even when there is mixing of the vibrational modes, it is generally possible to choose a single harmonic frequency that corresponds to each individual internal rotation. If, based on the internal modes analysis, there are two possible harmonic frequencies that correspond to a single internal rotation, we choose the lower vibrational frequency since these are generally associated with hindered rotors. Implicitly included in the process of calculating the HR corrected partition function is a consideration of the ZPE for each internal rotation. Since the energy levels for the 1-D hindered rotor partition function are not referenced to 0, the HR–ZPE is directly included in the partition function (given that the HR energy levels were calculated after setting $V(0)$ equal to the lowest energy). Barone [25] gave a nice discussion of how anharmonic motions affect the ZPE and Ellingson et al. [33] discuss various approximations to ZPE for separable and nonseparable cases.

[3] For example, the keyword "*freq = intmodes*" can be used in Gaussian 03 [2] to perform the internal modes analysis.

3 Alternatives and extensions of 1-D uncoupled rotation

3.1 Alternate model schemes

Treating anharmonicity and, in particular, internal rotation continues to be an area of active research, and there are a number of possible approaches put forth in the literature. Although the present work is a detailed overview of one popular approach, the 1-D hindered rotor model, we sought to put this model in context by giving a brief overview of several other methods. One important class of methods seeks improved accuracy by explicitly coupling internal and external rotation within a single rotational partition function [7,8,10]. These methods provide extremely accurate prediction of the

entropy and heat capacity and also give analytical expressions for the overall rotational partition function. This makes calculation of the density of states straightforward, and use of these methods dovetails well with RRKM theory (in which the density of states is explicitly required). In spite of the accuracy of these methods, their broad application is hindered by the complex algebra and extensive numerical integration required to calculate the partition functions [13]. Knyazev [13] quantified the impact of decoupling internal and external rotation, and Knyazev and Tsang [14] presented a straightforward algorithm for calculating partition functions and densities of states for 1-D nonharmonic degrees of freedom. Extensions of these methods are several approaches that employ Monte Carlo techniques for evaluating complex integrals found in more complex varieties of the partition functions [11,20,21,24,62,63]. These methods are all presented in the context of anharmonic motion within a well-behaved, e.g., sinusoidal, potential. The 1-D hindered rotor model and related methods, while limited in other areas, are formulated to be general for potentials of any shape. Additionally, the vibrational self-consistent field (VSCF) method can provide very accurate calculations of rotational–vibrational energies [37–41,64–66]. Treatment of torsional modes in transition states can also be treated via direct evaluation of a quantum-corrected classical phase space-based partition function [67,68].

3.2 Extension of the 1-DHR scheme to multiple rotors and other anharmonic degrees of freedom

The limitations of the 1-DHR model are well understood and have been discussed in detail elsewhere [26,29,47,56]. A major assumption which can lead to compromised accuracy of the 1-DHR model is that the potentials of the rotating tops within a single species are uncoupled with respect to the other internal rotations/vibrations. Van Speybroeck et al. [26] recently studied the thermochemistry of pentane and hexane and showed that cancellation of errors resulted in excellent agreement between the 1-DHR model and a fully coupled treatment for internal rotation. The effect of coupled internal rotations on calculated kinetic data has also been studied [9,18,29]. In essence, the approach to studying coupled internal rotations is similar to the 1-D approach. A two-dimensional (2-D) PES is generated for two rotations that are assumed a priori to be coupled, and a simple 2-D Hamiltonian similar in form to Eq. 1 is solved. The computational expense in this case increases dramatically since the PES which must be traversed in calculating the hindrance potentials becomes multi-dimensional. For example, studying two uncoupled 1-D internal rotations for 12 discrete angles requires only 24 constrained geometry optimizations, whereas calculating a 2-D PES for the same two rotations with the same degree of angular resolution for each rotation angle requires 144 constrained geometry optimizations. In addition, calculation of the energy levels for the subsequent coupled internal rotation is more complex. Thus, the application of coupled models to problems of engineering interest is currently limited.

In principle, other anharmonic motions such as puckering and inversion can be treated in an analogous manner to that outlined in Figs. 1 and 2. A corresponding 1-D anharmonic potential is determined for the motion under consideration along with an appropriate reduced moment of inertia, and Eq. 1 is solved analytically or numerically depending on the nature of the potential obtained. Katzer and Sax [28,4] gave an overall review of how many other anharmonic motions can be treated within the "1-D uncoupled motion" paradigm, and Vansteenkiste et al. [69] show application of this model to ring puckering in small cyclic compounds.

Finally, several methods have been offered to treat internal rotation that depart from the scheme described here, i.e., application of quantum mechanics to establish a hindrance potential and subsequent calculation of the energy levels for each rotation. Katzer and Sax [28] developed a method in which internal rotations are automatically identified from the geometry and Hessian, and the internal rotation partition functions are calculated using model potentials whose parameters are also informed by the calculation of the Hessian. This approach offers an economical and accurate route to approximating the contributions of internal rotation to the calculated partition functions and thermodynamic properties. Vansteenkiste et al. [32] have presented a new method, the extended hindered rotor model, that relies on separation of large amplitude motions from harmonic vibrations and also offers direct calculation of associated partition functions.

3.3 Probing 1-D uncoupled rotation

The remainder of this manuscript focuses on investigating aspects of the 1-DHR treatment which have not yet been examined quantitatively in the literature using representative calculations. Specifically, we have addressed what effect the type of optimization has when treating internal rotations of transition states. We have also explored the sensitivity of calculated properties of the hindered rotor to the choice of computational method/basis set used in establishing the hindrance potential. Finally, we have quantified the impact of the assumption that the reduced moment of inertia is invariant while rotating.

To probe these questions, we investigated two different systems. The first was the radical addition reaction

$$CH_3C \cdot HCl + C_2H_3Cl \rightarrow CH_3CHClCH_2C \cdot HCl$$

that is one of the first steps in poly(vinychloride) (PVC) polymerization. The complex hindrance potentials of the product, $CH_3CHClCH_2C \cdot HCl$, provide a nice opportunity to study the sensitivity of the calculated partition functions and thermodynamic properties to the step size used to calculate the potentials. The second reaction was the intramolecular hydrogen transfer reaction

$$(CH_3)_2CHO_2\cdot \rightarrow HO \cdot + CH_3COCH_3$$

that is a prototype reaction of an important reaction family in atmospheric chemistry. Note that the intramolecular product $CH_3C \cdot OOHCH_3$ is not observed, but rather the subsequent β-scission products are formed directly [70]. The insights derived from studying the transition states of these reactions are applicable to a wide range of related systems.

4 Computational and theoretical details

All MO and DFT calculations were completed using the Gaussian 03 [2] software package. The torsional hindrance potentials were calculated within Gaussian 03, and the partition functions and thermodynamic properties were calculated according to the method described in Sect. 2.1 which has been coded in the "Calctherm" and "Calck" software packages [51,52]. Calctherm and Calck provide partition functions, thermodynamic properties and TST rate constants that are fully corrected for internal rotation by first reading in structural and vibrational data from electronic structure software and then correcting internal rotations that have been identified by the user. The hindered rotor correction is performed by using the FGH method [61] to solve Eq. 1, and the energy levels for each internal rotation are used to calculate the partition function (Eq. 2) and associated thermodynamic properties (Eqs. 11 through 13). For all internal rotations and temperatures considered, kT was less than or approximately equal to the barrier height, V; thus the hindered rotor scheme was used for all corrections. Each internal rotation is processed to additively correct an entire species by (1) including the contribution to q, S, C_v, and E of each IR and (2) removing the corresponding contribution (within the HO approximation) for each low-frequency vibration matched to a hindered rotor. Calctherm is used to treat individual species, and Calck can be used to calculate rate coefficients, activation energies and pre-exponential factors using transition state theory. Molecular geometries were optimized using the B3LYP hybrid density functional [71] and the CBSB7 basis set that is represented as an extension of the Pople formalism as 6-311G(2d,d,p) and adds an additional 2d polarization function to third row atoms [72]. This is the basis set used in the hybrid model chemistry CBS-QB3 [72] which has been applied to study many problems of practical interest. Frequencies used in computing thermodynamic properties were scaled as recommended by Scott and Radom [73,72], i.e., 0.9806 for ZPE, 1.0015 for S_{vib}, and 0.9989 for H_{vib} and C_v. Additionally, for the study comparing methods and basis set we used MP2 and HF levels of theory with two additional basis sets, 3-21G and 6-31G(d).

5 Results and discussion

The optimized structures of the transition state and product from the PVC addition reaction and the transition state from the intramolecular hydrogen transfer reaction are shown in ball-and-stick format in Fig. 3. These are the structures that will be referred to in the sections below.

5.1 Calculation of the hindrance potential in transition states

Recently, we studied the intramolecular hydrogen transfer of a large number of alkylperoxy radicals [49]. These reactions proceed through a cyclic transition state before isomerizing to form a peroxy radical or peroxide moiety. As an approximation to aid in the calculation of hindrance potentials in the transition state, we simply chose to freeze all of the atoms which constituted the ring structure of the transition state. After freezing the coordinates in the ring, constrained geometry optimizations were performed to obtain the 1-D hindrance potentials for the remaining internal rotations. Rigorously, it is correct to calculate the partition function for the transition state, $Q^{\ddagger}(T)$, by identifying the saddle point at each point along the scan to obtain the hindrance potential. However, the additional computational demands imposed by this approach are significant, and we introduced this approximation to save computational cost. It would be reassuring to know that the simpler approach provides acceptable approximations to the more rigorous hindrance potentials.

To investigate the impact of the "frozen TS" assumption, we first located the transition state for both the radical addition and hydrogen transfer reactions. We then calculated the hindrance potential for the internal rotation(s) in each transition state using both methods: (1) re-optimizing the saddle point at each step, or (2) freezing the positions of the atoms defining the transition state to those occupied at $\theta = 0$. In the case of the radical addition reaction, the 4–3 bond length was frozen (structure "B", Fig. 3); for the intramolecular hydrogen transfer reaction, the bond lengths, bond angles and dihedral angles involving atoms 1, 2, 3, and 4 were frozen (structure "A", Fig. 3). For the sake of the comparisons done here, we treated motion about the TS bond in the radical addition reaction as an internal rotation as done by Izgorodina and Coote [54] and calculated a hindrance potential using the TS bond as the axis of rotation. For structure "A" in Fig. 3, we examined the 1–5 bond as the axis of rotation.

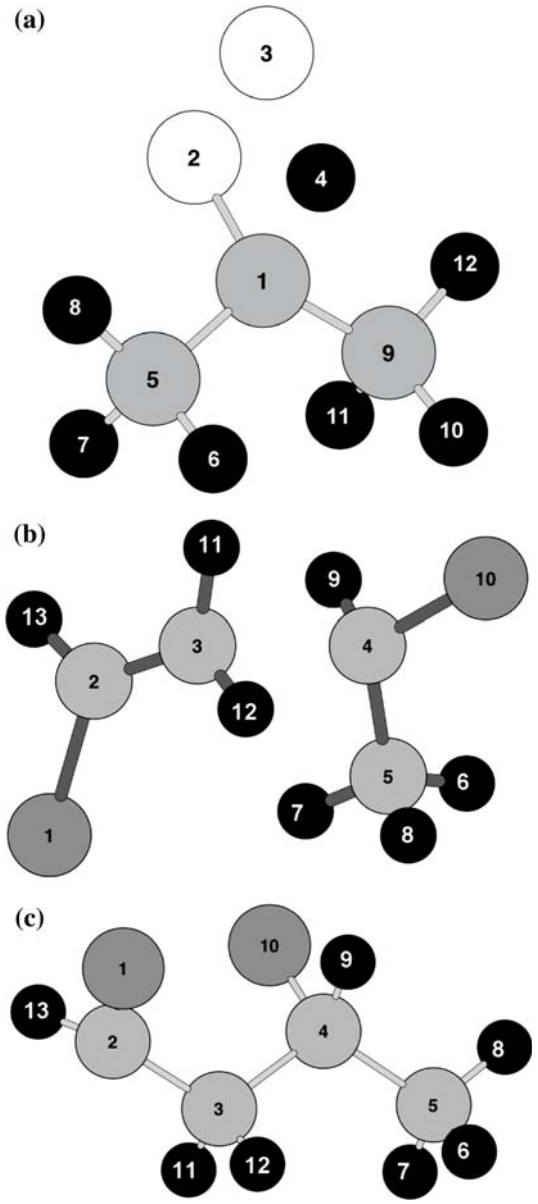

Fig. 3 Ball-and-stick diagrams of three compounds under consideration. Structure A is the transition state of a 1,3-hydrogen shift of 2-propyl peroxy radical. Structure B is the transition state for the first radical addition reaction in PVC polymerization. Structure C is the optimized product from the addition reaction of PVC. Carbon atoms are shown in *grey*; hydrogen atoms are shown in *black*; oxygen atoms are shown in *white*; and Cl atoms are shown in *dark grey*

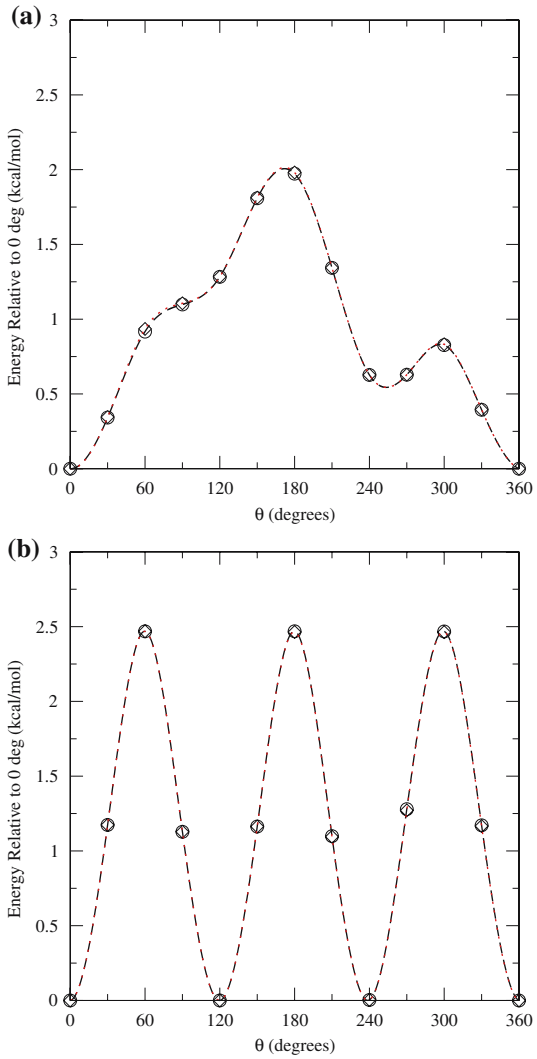

Fig. 4 Comparison of hindrance potential calculated for internal rotation in transition states calculated using two different approaches. Data calculated freezing the coordinates of the atoms defining the TS center are given with *open circles* and a *black dashed line*. Data calculated by re-optimizing the TS at each point throughout the rotation are shown as *open diamonds* and a *dotted line*. Each hindrance potential is calculated using 30° increments. **a** shows the results for rotating around the 4–3 bond in structure "B" of Fig. 3. **b** presents results for rotation around the 1–5 bond in structure "A" in Fig. 3

The results given in Fig. 4 show the hindrance potentials for the rotation about the 4–3 bond of the TS of the radical addition reaction (Fig. 4a; structure "B" in Fig. 3) and the rotation about the 1–5 bond of structure "A" in Fig. 3 (Fig. 4b) for the two different approaches. Remarkably, the hindrance potentials for the two methods are nearly indistinguishable, even for the much more complicated backbone rotation of the TS of the addition reaction. When Eq. 1 is solved with two identical potentials, the energy levels, partition functions and associated thermodynamic properties will also be identical. Although a limited sample was examined here, the results are encouraging that continued refinement of the atoms defining the transition state as θ is varied is not necessary. This offers a significant savings in computational time; the computational cost for establishing the hindrance potentials (using 30° increments) when the atoms defining the TS are frozen was roughly one-eighth that compared to re-optimization of the saddle point at each step for the two

cases examined here. For kinetic studies of large systems with many internal rotations or studies which involve many reactions, the advantage of the more simplified approach is clear. We note that if this approach is applied to transition states in which the transition state itself becomes an axis of rotation and there are also three atoms in the transition state moiety, e.g., intermolecular hydrogen transfer, it is not possible to simultaneously constrain (freeze) more than two out of four atoms that define a dihedral angle and subsequently scan that dihedral angle to obtain the hindrance potential. An alternate approach is suggested by Fernandez-Ramos et al. [67] in which the rate coefficients calculated at different torsional minima in the TS are summed.

5.2 Relating the choice of method and basis set to calculated properties of hindered rotors

An important question regarding use of the 1-DHR scheme is the choice of quantum method and basis set [9,69]. To probe the effect of this choice we examined the "4–3" backbone and "4–5" methyl group rotations of structure "C" in Fig. 3. To compare a variety of methods, we used HF, MP2, and B3LYP with three different basis sets 3-21G, 6-31G(d), and 6-311G(2d,d,p) (CBSB7). The hindrance potential was obtained by first optimizing each structure at the respective method/basis set combination and then scanning the rotation using 30° increments. It is interesting to compare the different hindrance potentials obtained to see their respective shapes and barrier heights as well as the impact these potentials have on the calculated properties. The calculated potentials are given in Fig. 5. The methyl group rotation is well behaved, and there is not much variability among methods and basis sets. However, some variability is seen for the "4–5" backbone rotation. For the medium and large basis sets, the barrier heights for all methods are in reasonable agreement. On the other hand, for all methods investigated, the 3-21G potentials for the backbone rotation (filled squares in panel A of Fig. 5) are qualitatively different from those obtained using 6-31G(d) or the CBSB7 basis sets. For the case of the HF/3-21G potential we note that periodic behavior was not obtained in the calculated potential unless we defined the "4–5" dihedral angle using H–C–C–H atoms.

The potentials shown in Fig. 5 for the nine different methods and basis set combinations were then used to calculate the hindered rotor partition function and hindered rotor entropy at 200 and 1,000 K. These data are given in Table 1. While the quantities obtained for each method (HF, MP2, or B3LYP) differ slightly in absolute magnitude, it is clear that the hindered rotor entropy is less sensitive to the size of the basis set than the partition function. These data give limited yet useful insight into the relative sensitivity of the calculated partition functions and entropy to method and basis set.

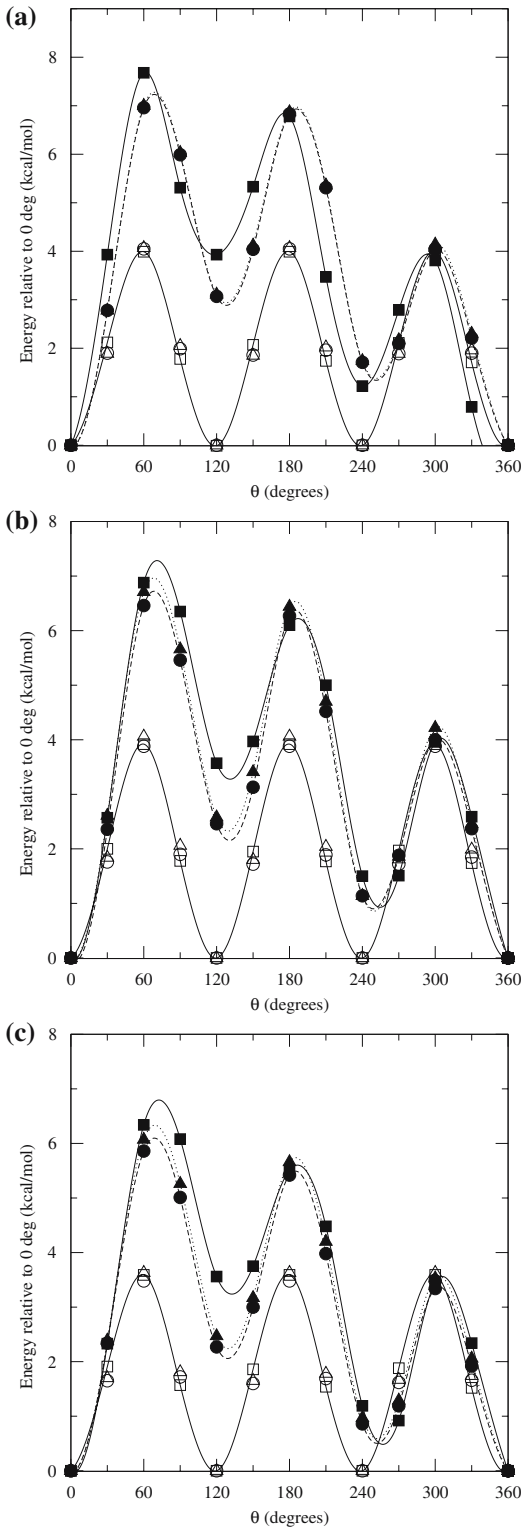

Fig. 5 Comparison of the hindrance potential calculated for the "4–3" (*closed symbols*) and "4–5" (*open symbols*) rotations in structure "C" of Fig. 3 using different methods and basis sets. The methods used were HF (panel **a**), MP2 (panel **b**), and B3LYP (panel **c**). The basis sets used were 3-21G (*squares*, *solid lines*), 6-31G(d) (*triangles*, *dotted lines*), and 6-311G(2d,d,p) (*circles*, *dashed lines*). To guide the eye, the fits for each data set in the "4–3" rotation are shown and only the data for the fit of the small basis set are shown for the "4–5"

Table 1 Calculated thermochemistry data for the potentials shown in Fig. 5

		3-21G		6-31G(d)		6-311G(2d,d,p)	
	T (K)	q_{hr}	S	q_{hr}	S	q_{hr}	S
HF	200	3.02	3.34	1.60	3.27	1.62	3.32
	1,000	17.01	8.27	15.58	8.38	15.87	8.40
MP2	200	1.75	3.60	1.76	3.70	1.82	3.70
	1,000	16.54	8.39	17.51	8.47	18.15	8.53
B3LYP	200	2.20	4.17	2.09	4.16	2.26	4.32
	1,000	18.77	8.46	19.84	8.58	20.89	8.63

The data given in the table are the hindered rotor partition function and entropy (cal/mol K)

5.3 Selection of appropriate step size while traversing hindrance potentials

Researchers who use the 1-DHR correction typically choose a step size between 10° and 30° in order to traverse the hindrance potential and establish $V(\theta)$. Obviously, this can vary the computational cost of a given study greatly given that these increments correspond to 37 and 13, respectively, constrained geometry optimizations in order to traverse one 360° rotation and ensure that the energies at the starting and ending points, i.e., 0° and 360°, are identical. To the best of our knowledge, there are no reported studies which probe the sensitivity of the calculated properties to this choice.

To study the effect of the fineness of the hindrance potential scan, we investigated the rotations of both the backbone (atoms 4 and 3 as the rotation axis) and the CHCl group (atoms 2 and 3 as the rotation axis) in the product of the radical addition reaction shown as structure "C" in Fig. 3. The "4–5" rotation is very well behaved so no comparison using different step sizes is provided. Using B3LYP/CBSB7, step sizes of 1°, 15°, 30°, and 40° were used for each rotation, and the data were fit to a full Fourier series using 10, 10, 10, or 8 coefficients, respectively. The Fourier coefficients are given in Table 1 of the Supplementary Information for reference, and the calculated data and best fits are plotted in Fig. 6. The plot in Fig. 6a shows that for the more complicated backbone rotation (bond "4–3"), all of the data are essentially in perfect agreement. It is a bit surprising that the 40° scan which uses only eight terms in the Fourier series is able to perfectly capture the data from the much more computationally expensive 1° scan. It is also interesting that even though the scan in increments of 40° has points which are substantially further (as compared to the 1°, 15° and 30° scans) from the three peaks in energy, the fitted terms can still capture the data as well as the finer scans. This good agreement is very encouraging given the complexity involved with this and other backbone rotations. The "2–3" rotation of the CHCl group is less regular than the backbone rotation

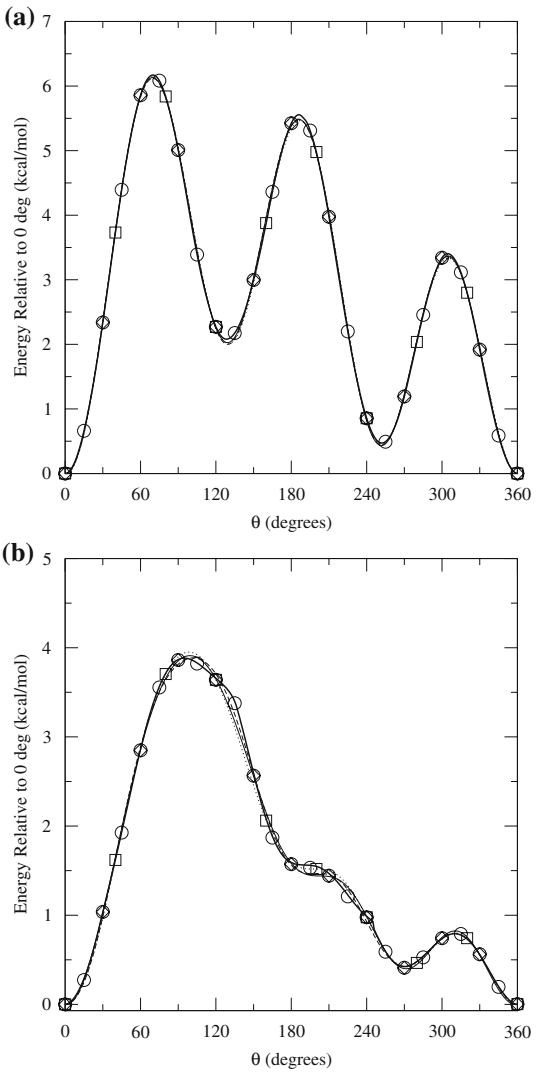

Fig. 6 Comparison of hindrance potential (kcal/mol) and corresponding Fourier series fits calculated for the "4–3" (**a**) and "2–3" (**b**) rotations in structure "C" of Fig. 3. The potentials were calculated by traversing a step size of 1° (*heavy solid line*), 15° (*circles/solid line*), 30° (*diamonds/dashed line*), and 40° (*squares/dotted line*). For the 1° step size, the actual data from electronic structure calculations are shown as a single line. The coefficients for the Fourier series are given in the Supplementary Information

as shown in Fig. 6b. However, all four scans are in very good agreement. We found that it in order to obtain meaningful results, it was necessary to define the dihedral angle using the C–C–C–Cl atoms. If other combinations of atoms were used, a sharp peak was observed when the C and Cl (atoms 4 and 1) were perfectly eclipsed.

It was therefore interesting to calculate what impact these discrepancies had on thermodynamic properties. We calculated the entropy, heat capacity and the thermal contribution to the internal energy for these two rotations ("2–3" and "4–3") using the energy levels obtained from solution of Eq. 1. The calculated entropy, heat capacity, and

Table 2 Calculated thermochemistry data for the potentials shown in Fig. 6

T (K)	1° scan			15° scan			30° scan			40° scan			Harmonic oscillator		
	S	C_v	E	S	C_v	E	S	C_v	E	S	C_v	E	S	C_v	E
Rotation about the "4–3" backbone C–C bond. $\nu = 84.4\,\mathrm{cm}^{-1}$															
200	4.74	0.53	2.78	4.74	0.53	2.78	4.74	0.54	2.80	4.72	0.54	2.84	2.92	6.83	0.41
400	6.74	1.11	2.92	6.74	1.11	2.92	6.74	1.12	2.92	6.74	1.12	2.94	4.27	3.71	0.80
600	7.87	1.67	2.63	7.87	1.67	2.63	7.88	1.67	2.63	7.88	1.68	2.63	5.07	3.02	1.19
800	8.58	2.16	2.28	8.58	2.16	2.28	8.58	2.16	2.27	8.59	2.17	2.27	5.64	2.72	1.59
1,000	9.06	2.59	1.99	9.06	2.59	1.99	9.06	2.59	1.98	9.06	2.59	1.98	6.09	2.56	1.99
Rotation about the "2–3" C–C bond. $\nu = 48.6\,\mathrm{cm}^{-1}$															
200	5.04	0.57	2.50	5.06	0.57	2.49	5.03	0.56	2.52	5.04	0.57	2.51	4.16	3.85	0.40
400	6.59	1.01	2.01	6.60	1.01	2.00	6.59	1.01	2.03	6.60	1.01	2.03	5.53	2.77	0.80
600	7.36	1.38	1.77	7.36	1.38	1.76	7.36	1.39	1.77	7.37	1.39	1.77	6.33	2.48	1.19
800	7.84	1.72	1.58	7.84	1.72	1.57	7.85	1.72	1.58	7.85	1.72	1.57	6.91	2.35	1.59
1,000	8.18	2.02	1.44	8.18	2.02	1.44	8.18	2.02	1.44	8.18	2.02	1.43	7.35	2.27	1.99

The data given in the table are the entropy (cal/mol K), heat capacity (cal/mol K) and internal energy (kcal/mol)[a]. Both rotations were calculated to be hindered rotors over the temperature range considered. The values based on the harmonic oscillator approximation[b] (including ZPE) are given for reference[c]. The frequency assigned to each internal rotation is given in the table

[a] The thermal contribution to the internal energy is calculated as $E = RT^2 \left(\frac{\partial \ln q}{\partial T}\right)_V$. The total internal energy is not reported since it includes the electronic energy which is very large compared to the values reported here. The energy levels for the hindered rotor include the ZPE, i.e., the ground-state energy is not 0; therefore the HO values include the ZPE, $\frac{1}{2}h\nu$, for fair comparison

[b] Following the recommendation of Scott and Radom [73], the frequencies were scaled by 1.0015 (calculation of entropy), 0.9989 (calculation of $E_{\mathrm{vib}}^{\mathrm{HO}}$), 0.9806 (ZPE), and 0.9989 (C_v)

[c] There are three low-frequency vibrations which could potentially be assigned to the two rotations ("4–3" and "2–3"). Normal mode analysis reveals the contributions of these backbone rotations to each of the frequencies as: 48.6 cm^{-1} ["2–3" : 54.7%, "4–3" : 35.3%], 88.2 cm^{-1} ["2–3" : 35.3%, "4–3" : 52.7%], 190.4 cm^{-1} ["2–3" : 63.1%, "4–3" : 11%]. For illustration purposes, we chose the two lowest frequencies to assign as hindered rotors, although the mixing of vibrational modes is known to present difficulties [30]

internal thermal energy for the temperature range 200 to 1,000 K are given in Table 2. As expected all of the data agree well for both internal rotations given the similarities in the hindrance potentials that were fit. The data for the 40° scans of both rotations agree surprisingly well with the 1° data, demonstrating that any minor deviations between the fit hindrance potentials as shown in Fig. 6 do not affect the calculated thermodynamic properties substantially. In generalizing these results to complex molecules with many internal rotations, it should be remembered that small deviations for each internal rotation may result in significant deviations for the property of a species as a whole since the contributions are additive. Finally, the data in Table 2 also include the corresponding harmonic oscillator data if one were to simply use the HO approximation for all calculations. The comparison between all four step sizes and the HO data clearly shows strong deviation between the HO approximation and the 1-DHR correction.

Calculations such as the type illustrated in Fig. 6 and Table 2 are helpful because they offer a rational template for deciding how much computational resource to expend while exploring the hindrance potential and performing the 1-DHR correction. Especially given the complex, asymmetric rotation potentials produced by the bulky chlorine atoms, these results should give insight for a wide range of systems. To our knowledge, these results are the first systematic, quantitative comparison of using different step sizes for the constrained geometry optimization.

5.4 Investigation of the reduced moment of inertia as a function of the rotation angle

In spite of the importance of the reduced moment of inertia in calculating the 1-DHR correction, there are no reported studies quantifying I_{red} as a function of θ for bulky, asymmetric groups, although East and Radom [9] probed the sensitivity of calculated entropy values to changes in I_{red} within the Pitzer-Gwinn formalism. One potential solution is to calculate the reduced moment of inertia for a top using the formulae in Sect. 2.1.2 as a function of θ, fit the data to a functional form, and then use that function in solving the energy levels for the rotating top [56]. Further work must be done, however, to assess (1) the degree to which I_{red} changes as an asymmetric top rotates and (2) the degree to which these changes impact the partition function and calculated thermodynamic properties.

One final consideration in examining the accuracy of the 1-DHR calculation is the degree to which the reduced moment

of inertia changes as a function of the dihedral angle that specifies a given internal rotation. The relaxation of the structure subject to (1) the constraint of the fixed dihedral angle and possibly (2) the constraint to freeze the atoms defining the transition state could result in changes in I_{red} as a function of rotation. To investigate this, each dihedral angle (bonds "2–3", "4–3" and "4–5") in the product of the PVC addition reaction, structure "C" in Fig. 3, was scanned in 30° increments. Each scan has 13 steps, thereby giving 13 distinct optimized geometries, and the reduced moment of inertia for each particular rotation bond was calculated for each of the 13 structures, affording I_{red} as a function of the angle of rotation. We calculated all three of the different $I^{2,n}$ presented in Sect. 2.1.2, and these data are summarized graphically in Fig. 7.

The rotation involving the methyl group, as expected, has a nearly constant reduced moment of inertia as a function of rotation angle. In addition, the three $I^{2,n}$ all give roughly the same value for the rotation of the methyl group. The values of $I^{2,n}$ for the backbone ("4–3"' bond) and CHCl ("2–3" bond) rotations are very different and follow the expected trend, i.e., $I^{2,1} > I^{2,2} > I^{2,3}$. To help understand the large differences between the various $I^{2,n}$ shown in Fig. 7, it is helpful to remember that the reduced moment of inertia combines the moments for each of the "tops" and that each top contains a single heavy chlorine atom. It is therefore not surprising that such large and disparate I_{red} values are obtained given their strong dependence on the square of the Cl-*axis of rotation* distance. It is interesting to observe that for the approximations $n = 1$ and $n = 2$ (panel a and panel b, respectively) in Fig. 7, the reduced moments of inertia are essentially constant as the dihedral angle is scanned. We hypothesize that this is because the axis of rotation is either fixed ($n = 1$) or can move but stays parallel to the single bond connecting the rotating groups ($n = 2$). For the third approximation of rotor-rotor coupling ($n = 3$), the axis of rotation is only defined by the two centers of mass and can vary greatly as the dihedral angle is scanned. Therefore, the distance between the Cl atoms and the axis of rotation can change much more and make a stronger impact on the effective moment of inertia. Examining panel c in Fig. 7 shows that dramatic changes are seen in the reduced moment of inertia as a function of angle for the backbone rotation ("4–3" bond) and the rotation of the CHCl group ("2–3" bond). The stationary points have reduced moments of inertia of 31.1 amu Å^2 ("4–3") and 14.1 amu Å^2 ("2–3"), but the range of values for the two rotations is 22–39 amu Å^2 ("4–3") and 4–21 amu Å^2 ("2–3") as the angle is changed from 0° to 360°.

The rotation about the "2–3" bond was used to probe the sensitivity of changes in I_{red} to calculated properties because it is one of the rotations that has the largest changes in the reduced moment of inertia as a function of θ. As a first approximation, we solved Eq. 1 by using the same rotational

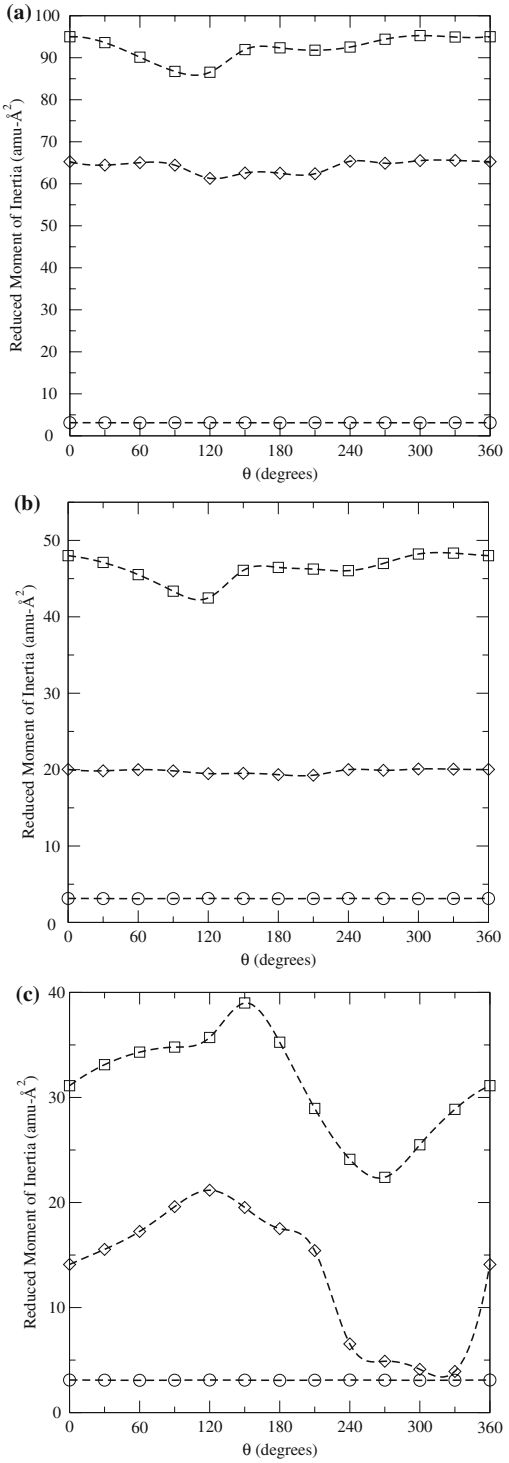

Fig. 7 Comparison of the reduced moment of inertia as a function of rotation angle for each of three different rotating tops in structure "C" in Fig. 3 calculated according to the prescription in Sect. 2.1.2. The data are calculated using three different approximations of rotor-rotor coupling: $I^{2,1}$ (panel **a**), $I^{2,2}$ (panel **b**), and $I^{2,3}$ (panel **c**). The data in the figure show the reduced moment of inertia calculated in 30° increments. The "4–5" (methyl group) rotation is denoted by *open circles*, the "4–3" (backbone) rotation is shown with *squares*, and the "2–3" (CHCl) group is denoted by *open diamonds*. A cubic spline (*dashed line*) is drawn for each data set for reference

potential and systematically changed its value between 4 and 21 amu Å^2 in order to explore the sensitivity of the partition function and thermodynamic properties to the value of I_{red}. The calculated partition function and entropy at 298.15 K are given in Table 3. Within the 1-DHR approximation, the large relative changes in the reduced moment of inertia can have a meaningful impact on the calculated thermodynamic properties. The partition function is seen to change from approximately −47 to +22% of its value at the equilibrium structure and the entropy changes are less drastic varying from −20 to +6% of their equilibrium values. Additionally, we found that the calculated changes in q_{hr} and S vary only a small amount as a function of temperature.

It is interesting to compare these calculated results to the results of East and Radom [9] who also studied the sensitivity of the calculated entropy to changes in the reduced moment of inertia. Within the Pitzer and Gwinn formalism, they varied the height of the rotational potential for a top with symmetry number (σ_r) of three between 0.96 and 2.63 kcal/mol, and the reduced moment of inertia was changed between 0.65 and 3.0 amu Å^2. Their results show the calculated entropy to be strongly dependent on both terms. This is consistent with the results given in Table 3 since the hindered rotor entropy was observed to be dependent on the reduced moment of inertia for the PVC radical product. For example, the data from East and Radom show that an increase by a factor of 4.6 in I_{red} corresponds to an increase of 1.5 cal/mol K in the hindered rotor entropy, and an increase of a factor of 5 (changing from 4 to 20) in I_{red} from the data in Table 3 corresponds to an increase of 1.6 cal/mol K in the hindered rotor entropy. To explore this further, we compared the results of East and Radom in terms of S versus I_{red} as a function of V/RT, where V is the barrier to rotation, with results from our method for V/RT of 1.6, 4.4, and 10. The values V/RT = 1.6 and 4.4 correspond to those chosen by East and Radom in their study, and the value of V/RT = 10 was chosen because it represents a barrier height of 6 kcal/mol at 298.15 K which is the barrier height of the "4–3" rotation in the product of the PVC addition reaction (see Fig. 6a). The calculated data are summarized graphically in Fig. 8 using a logarithmic axis for I_{red} since the entropy is dependent on the logarithm of the reduced moment of inertia.

The data presented here show that the main consideration in studying the effect of changes in I_{red} as a function of the rotation angle is the relative difference and not the absolute difference. For example, the data in Table 3 shows that changing I_{red} from 14.1 to 20 amu Å^2 changes the entropy by only 0.39 cal/mol K where as a comparable absolute change in the regime explored by East and Radom (changing I_{red} from 0.65 to 5.65 amu Å^2) causes a change in the entropy of 2.07 cal/mol K. Although these results are given for symmetric tops, the conclusions are general for tops of any symmetry number. Manipulation of Eq. 11 shows that for tops with a symmetry number greater than one the hindered rotor entropy is uniformly decreased by the quantity $k \ln \sigma_{r_i}$. Thus, the trend of the curves shown in Fig. 8 is invariant with the internal symmetry number of the top. These results are important in the development of heuristics for using the 1-DHR model. If the relative changes in I_{red} as a function of the rotation angle are not large, then accurate properties are still obtained using the 1-DHR model.

Table 3 Calculated partition function and entropy (cal/mol K) for the rotation "2-3" of structure "C" in Fig. 3

I_{red}	q_{hr}	S
4	3.39	4.94
10	5.38	5.85
14.1[a]	6.39	6.19
20	7.61	6.53
21	7.80	6.58

The reduced moment of inertia (amu Å^2) is given for reference and adjusted to cover the full range seen in this rotation, as shown in Fig. 7c. The data are calculated at 298.15 K

[a] The reduced moment of inertia calculated at the minimum energy structure

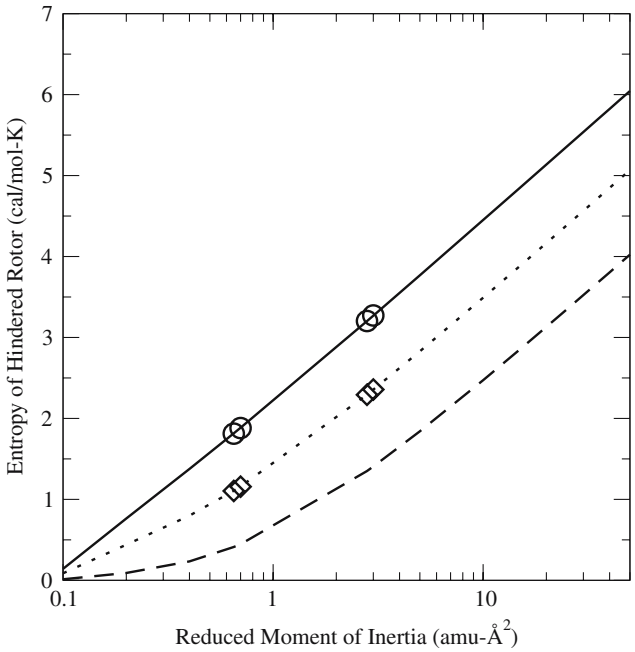

Fig. 8 Comparison of the hindered rotor entropy with changes in the reduced moment of inertia for several different potentials of varying V/RT. The data are calculated at 298.15 K and all potentials represent a top with a rotational symmetry number (σ_r) of three. The *symbols* are taken from East and Radom [9] and the data in *lines* are calculated using the approach given in this paper and the Calctherm software. The potentials considered V/RT = 1.6 (*open circles*, *solid line*), 4.4 (*open diamonds*, *dotted line*), and 10 (*dashed line*)

6 Summary and future outlook

We have given an overview of how the 1-DHR scheme can be used to treat internal rotation. Additionally, we have sought to put the 1-DHR scheme in context by providing a brief summary of the current practice in quantum-mechanical treatment of internal rotation. The uncoupled, 1-D hindered rotor model has been widely applied to study numerous problems of chemical and engineering interest. We expect the 1-DHR model to continue to be a general part of the modeling toolkit for ab initio studies since there are few alternatives to the 1-DHR model that are both computationally tractable and general for tops of any symmetry. In response to the lack of general electronic structure codes that make the 1-DHR model part of the standard menu of choices, we have offered two codes, "Calctherm" and "Calck", that extract data from electronic structure software output, perform the 1-DHR correction, and finally output thermodynamic and kinetic properties which have been fully corrected for internal rotation.

Several calculations were performed to test the applicability of the 1-DHR model to a wide range of systems and revealed how the 1-DHR model may be more efficiently applied in general. We have shown that rotational hindrance potentials in the transition state can be determined by simply freezing the atoms defining the transition state instead of re-optimizing to a transition state at each point throughout the rotation. Additionally, we have explored the sensitivity of calculated properties to the choice of step size (in scanning each rotational top) and the method and basis set. These results can help modelers make rational choices and realize significant savings in computational cost when applying the 1-DHR model. Finally, we used highly asymmetric rotating tops to quantify how much the reduced moment of inertia changes as it undergoes rotation. The sensitivity of calculated properties to the changes in the reduced moment of inertia was calculated, and we showed that in general changes in the reduced moment of inertia do not compromise the accuracy of the 1-DHR model.

Acknowledgments This work was partially supported by the NSF IGERT program (award number: DGE-0114429) and the National Center for Supercomputing Applications under TG-CTS050021 utilizing the Pittsburgh Supercomputing Center. Support from the Inter-American Materials Collaboration Program of the National Science Foundation (DMR-0303435) is also acknowledged. We are grateful for helpful discussions with Dr. Veronique Van Speybroeck.

References

1. Schmidt M, Baldridge K, Boatz JA, Elbert S, Gordon MS, Jensen J, Koseki S, Matsunaga N, Nguyen K, Su S, Windus T, Dupuis M, Montgomery JA (1993) General atomic and molecular electronic structure system. J Comp Chem 14:1347–1363
2. Frisch MJ, Trucks GW, Schlegel HB, Scuseria GE, Robb MA, Cheeseman JR, Montgomery JA Jr, Vreven T, Kudin KN, Burant JC, Millam JM, Iyengar SS, Tomasi J, Barone V, Mennucci B, Cossi M, Scalmani G, Rega N, Petersson GA, Nakatsuji H, Hada M, Ehara M, Toyota K, Fukuda R, Hasegawa J, Ishida M, Nakajima T, Honda Y, Kitao O, Nakai H, Klene M, Li X, Knox JE, Hratchian HP, Cross JB, Bakken V, Adamo C, Jaramillo J, Gomperts R, Stratmann RE, Yazyev O, Austin AJ, Cammi R, Pomelli C, Ochterski JW, Ayala PY, Morokuma K, Voth GA, Salvador P, Dannenberg JJ, Zakrzewski VG, Dapprich S, Daniels AD, Strain MC, Farkas O, Malick DK, Rabuck AD, Raghavachari K, Foresman JB, Ortiz JV, Cui Q, Baboul AG, Clifford S, Cioslowski J, Stefanov BB, Liu G, Liashenko A, Piskorz P, Komaromi I, Martin RL, Fox DJ, Keith T, Al-Laham MA, Peng CY, Nanayakkara A, Challacombe M, Gill PMW, Johnson B, Chen W, Wong MW, Gonzalez C, Pople JA (2003) Gaussian 03, Revision C.02. Gaussian Inc., Wallingford, 2004
3. Pitzer KS, Gwinn WD (1942) Energy levels and thermodynamic functions for molecules with internal rotation. I. Rigid frame with attached tops. J Chem Phys 10(7):428–440
4. Katzer G, Sax AF (2002) Beyond the harmonic approximation: Impact of anharmonic molecular vibrations on the thermochemistry of silicon hydrides. J Phys Chem A 106(31):7204–7215
5. Isaacson AD, Truhlar DG (1981) The accuracy of the Pitzer-Gwinn method for partition-functions of anharmonic vibrational-modes. J Chem Phys 75(8):4090–4094
6. Truhlar DG (1991) A simple approximation for the vibrational partition function of a hindered internal rotation. J Comp Chem 12(2):266–270
7. Aubanel EE, Robertson SH, Wardlaw DM (1991) Hindered rotor model for radical association reactions. J Chem Soc Faraday T 87(15):2291–2297
8. Gang J, Pilling MJ, Robertson SH (1996) Partition functions and densities of states for butane and pentane. J Chem Soc Faraday Trans 92(19):3509–3518
9. East ALL, Radom L (1997) Ab initio statistical thermodynamical models for the computation of third-law entropies. J Chem Phys 106(16):6655–6674
10. Gang J, Pilling MJ, Robertson SH (1997) Asymmetric internal rotation: Application to the $2\text{-}C_4H_9 \rightleftharpoons CH_3 + C_3H_6$ reaction. J Chem Soc Faraday Trans 93(8):1481–1491
11. Gang J, Pilling MJ, Robertson SH (1998) Monte Carlo calculation of partition functions for straight chain alkanes. Chem Phys 231 (2–3):183–192
12. Ayala PY, Schlegel HB (1998) Identification and treatment of internal rotation in normal mode vibrational analysis. J Chem Phys 108(6):2314–2325
13. Knyazev VD (1998) Density of states of one-dimensional hindered internal rotors and separability of rotational degrees of freedom. J Phys Chem A 102(22):3916–3922
14. Knyazev VD, Tsang W (1998) Nonharmonic degrees of freedom: densities of states and thermodynamic functions. J Phys Chem A 102(46):9167–9176
15. Chen CJ, Bozzelli JW (1999) Analysis of tertiary butyl radical plus O_2, isobutene plus HO_2, isobutene plus OH, and isobutene-OH adducts plus O_2: a detailed tertiary butyl oxidation mechanism. J Phys Chem A 103(48):9731–9769
16. Van Speybroeck V, Van Neck D, Waroquier M, Wauters S, Saeys M, Marin GB (2000) Ab initio study of radical addition reactions: addition of a primary ethylbenzene radical to ethene. J Phys Chem A 104(46):10939–10950
17. Chuang YY, Truhlar DG (2000) Statistical thermodynamics of bond torsional modes. J Chem Phys 112(3):1221–1228
18. Van Speybroeck V, Van Neck D, Waroquier M (2002) Ab initio study of radical reactions: role of coupled internal rotations on the reaction kinetics (III). J Phys Chem A 106(38):8945–8950

19. Katzer G, Sax AF (2002) Numerical determination of pseudorotation constants. J Chem Phys 117(8):8219–8228
20. Miller TF, Clary DC (2002) Torsional path integral Monte Carlo method for the quantum simulation of large molecules. J Chem Phys 116(19):8262–8269
21. Miller TF, Clary DC (2003) Torsional path integral Monte Carlo method for calculating the absolute quantum free energy of large molecules. J Chem Phys 119(1):68–76
22. Katzer G, Sax AF (2003) A novel partition function for partially asymmetrical internal rotation. Chem Phys Lett 368(3–4):473–479
23. Vansteenkiste P, Van Speybroeck V, Marin GB, Waroquier M (2003) Ab initio calculation of entropy and heat capacity of gas-phase *n*-alkanes using internal rotations. J Phys Chem A 107(17):3139–3145
24. Lynch VA, Mielke SL, Truhlar DG (2004) Accurate vibrational-rotational partition functions and standard-state free energy values for H_2O_2 from Monte Carlo path-integral calculations. J Chem Phys 121(11):5148–5162
25. Barone V (2004) Vibrational zero-point energies and thermodynamic functions beyond the harmonic approximation. J Chem Phys 120(7):3059–3065
26. Van Speybroeck V, Vansteenkiste P, Van Neck D, Waroquier M (2005) Why does the uncoupled hindered rotor model work well for the thermodynamics of *n*-alkanes. Chem Phys Lett 402:479–484
27. Sebbarand N, Bockhorn H, Bozzelli JW (2005) Thermochemical properties, rotation barriers, and group additivity for unsaturated oxygenated hydrocarbons and radicals resulting from reaction of vinyl and phenyl radical systems with O_2. J Phys Chem A 109(10):2233–2253
28. Katzer G, Sax AF (2005) Identification and thermodynamic treatment of several types of large-amplitude motions. J Comput Chem 26(14):1438–1451
29. Wong BM, Green WH Jr (2005) Effects of large-amplitude torsions on partition functions: Beyond the conventional separability assumption. Mol Phys 103(6–8):1027–1034
30. Van Cauter K, Van Speybroeck V, Vansteenkiste P, Reyniers MF, Waroquier M (2006) Ab initio study of free-radical polymerization: polyethylene propagation kinetics. Chem Phys Chem 7(1):131–140
31. Lynch VA, Mielke SL, Truhlar DG (2006) High-precision quantum thermochemistry on nonquasiharmonic potentials: converged path-integral free energies and a systematically convergent family of generalized Pitzer-Gwinn approximations. J Phys Chem A 110(17):5965–5965
32. Vansteenkiste P, Van Neck D, Van Speybroeck V, Waroquier M (2006) An extended hindered-rotor model with incorporation of Coriolis and vibrational-rotational coupling for calculating partition functions and derived quantities. J Chem Phys 124(4) Art. No. 044314
33. Ellingson BA, Lynch VA, Mielke SL, Truhlar DG (2006) Statistical thermodynamics of bond torsional modes: Tests of separable, almost-separable, and improved Pitzer-Gwinn approximations. J Chem Phys 125(8):084305
34. da Silva G, Kim CH, Bozzelli JW (2006) Thermodynamic properties (enthalpy, bond energy, entropy, and heat capacity) and internal rotor potentials of vinyl alcohol, methyl vinyl ether, and their corresponding radicals. J Phys Chem A 110(25):7925–7934
35. Wong BM, Thom RL, Field RW (2006) Accurate inertias for large-amplitude motions: improvements on prevailing approximations. J Phys Chem A 110(23):7406–7413
36. McClurg RB, Flagan RC, Goddard WA (1997) The hindered rotor density-of-states interpolation function. J Chem Phys 16(2):6675–6680
37. Bowman JM (1986) The self-consistent-field approach to polyatomic vibrations. Acc Chem Res 19(7):202–208
38. Handy NC (1987) The derivation of vibration-rotation kinetic-energy operators, in internal coordinates. Mol Phys 61(1):207–223
39. Carter S, Bowman JM, Handy NC (1998) Extensions and tests of 'multimodes': a code to obtain accurate vibration/rotation energies of many-mode molecules. Theor Chem Acc 100(1–4):191–198
40. Handy NC, Carter S (2004) Large vibrational variational calculations using 'multimode' and an iterative diagonalization technique. Mol Phys 102(21–22):2201–2205
41. Carter S, Handy NC, Tarroni R (2005) A variational method for the calculation of spin-rovibronic energy levels of any triatomic molecule in an electronic triplet state. Mol Phys 103(6–8):1131–1137
42. Pitzer KS (1946) Energy levels and thermodynamic functions for molecules with internal rotation. II Unsymmetrical tops attached to a rigid frame. J Chem Phys 14(4):239–243
43. Kilpatrick JE, Pitzer KS (1949) Energy levels and thermodynamic functions for molecules with internal rotation. III Compound rotation. J Chem Phys 17(11):1064–1075
44. Sumathi R, Green WH Jr (2002) Missing thermochemical groups for large unsaturated hydrocarbons: Contrasting predictions of G2 and CBS-Q. J Phys Chem A 106:11141–11149
45. Gomez-Balderas R, Coote ML, Hendry D, Radom L (2004) Reliable theoretical procedures for calculating the rate of methyl radical addition to carbon-carbon double and triple bonds. J Phys Chem A 108(15):2874–2883
46. Coote ML, Wood GPF, Radom L (2002) Methyl radical addition to C=S double bonds: Kinetic versus thermodynamic preferences. J Phys Chem A 106(50):12124–12138
47. Sumathi R, Carstensen HH, Green WH Jr (2001) Reaction rate prediction via group additivity Part 1: H abstraction from alkanes by H and CH_3. J Phys Chem A 105(28):6910–6925
48. Heuts JPA, Gilbert RG, Radom L (1996) Determination of Arrhenius parameters for propagation in free-radical polymerizations: an assessment of ab initio procedures. J Phys Chem 100(49):18997–19006
49. Pfaendtner J, Yu X, Broadbelt LJ (2006) Quantum chemical investigation of low-temperature intramolecular hydrogen transfer reactions of hydrocarbons. J Phys Chem A 110(37):10863–10871
50. McQuarrie DA, Simon JD (1999) Molecular thermodynamics. University Science Books, Sausalito
51. Pfaendtner J, Yu X, Broadbelt LJ (2006) Calctherm version 0.9. http://broadbelt.chem-eng.northwestern.edu
52. Pfaendtner J, Yu X, Broadbelt LJ (2006) Calck version 0.9. http://broadbelt.chem-eng.northwestern.edu
53. Wijaya C, Sumathi R, Green WH Jr (2003) Thermodynamic properties and kinetic parameters for cyclic ether formation from hydroperoxyalkyl radicals. J Phys Chem A 107(24):4908–4920
54. Izgorodina EI, Coote ML (2006) Accurate ab initio prediction of propagation rate coefficients in free-radical polymerization: acrylonitrile and vinyl chloride. J Chem Phys 324(1):96–110
55. Herschbach DR, Johnston HS, Pitzer KS, Powell RE (1956) Theoretical pre-exponential factors for 12 bimolecular reactions. J Chem Phys 25(4):736–741
56. Sumathi R, Green WH Jr (2002) A priori rate constants for kinetic modeling. Theor Chem Acc 108(4):187–213
57. Carbonniere P, Barone V (2004) Coriolis couplings in variational computations of vibrational spectra beyond the harmonic approximation: implementation and validation. Chem Phys Lett 392(4–6):365–371
58. Nordholm S, Bacskay G (1976) Generalized finite-element method applied to bound-state calculation. Chem Phys Lett 42(2):253–258
59. Balint-Kurti GG, Dixon R, Marston CC (1992) Grid methods for solving the Schrödinger equation and time dependent quantum dynamics of molecular photofragmentation and reactive scattering processes. Int Rev Phys Chem 11:317–344

60. Balint-Kurti GG, Ward CL, Marston CC (1991) Two computer programs for solving the Schrödinger equation for bound state eigenvalues and eigenfunctions using the Fourier grid Hamiltonian method. Comput Phys Commun 67:285–292
61. Marston CC, Balint-Kurti GG (1989) The Fourier grid Hamiltonian method for bound state eigenvalues and eigenfunctions. J Chem Phys 91(6):3571–3576
62. Tafipolsky M, Schmid R (2005) Calculation of rotational partition functions by an efficient Monte Carlo importance sampling technique. J Comput Chem 26(15):1579–1591
63. Chempath S, Predescu C, Bell AT (2006) Quantum mechanical single molecule partition function from path integral Monte Carlo simulations. J Chem Phys 124(23):234104
64. Carter S, Culik SJ, Bowman JM (1997) Vibrational self-consistent field method for many-mode systems: a new approach and application to the vibrations of CO adsorbed on Cu(100). J Chem Phys 107(24):10458–10469
65. Carter S, Bowman JM (1998) The adiabatic rotation approximation for rovibrational energies of many-mode systems: description and tests of the method. J Chem Phys 108(11):4397–4404
66. Bowman JM, Carter S, Huang XC (2003) Multimode: a code to calculate rovibrational energies of polyatomic molecules. Int Rev Phys Chem 22(3):533–549
67. Fernandez-Ramos A, Miller JA, Klippenstein SJ, Truhlar DG (2006) Modeling the kinetics of bimolecular reactions. Chem Rev 106(11):4518–4584
68. Greenwald EE, North SW, Georgievskii Y, Klippenstein SJ (2005) A two transition state model for radical-molecule reactions: a case study of the addition of OH to C_2H_4. J Phys Chem A 109(27):6031–6044
69. Vansteenkiste P, VanSpeybroeck V, Verniest G, DeKimpe N, Waroquier M (2006) Applicability of the hindered rotor scheme to the puckering mode in four-membered rings. J Phys Chem A 110(10):3838–3844
70. Denisova TG, Denisov ET (2001) Kinetic parameters of alkyl, alkoxy, and peroxy radical isomerization. Kinet Catal 42(5):620–630
71. Becke AD (1993) Density-functional thermochemistry 3. The role of exact exchange. J Chem Phys 98(7):5648–5652
72. Montgomery JA, Frisch MJ, Ochterski JW, Petersson GA (1999) A complete basis set model chemistry. VI. Use of density functional geometries and frequencies. J Chem Phys 110(6):2822–2827
73. Scott A, Radom L (1996) Harmonic vibrational frequencies: an evaluation of Hartree-Fock, Møller-Plesset, quadratic configuration interaction, density functional theory, and semiempirical scale factors. J Phys Chem 100(41):16502–16513